Hindawi
Advances in Astronomy
Volume 2018, Article ID 4575679, 13 pages
https://doi.org/10.1155/2018/4575679

Research Article

A Novel Scanning Method Applied to New-Style Solar Telescope Based on Autoguiding System

Zhi-ming Song[1,2] **and Zhong-quan Qu**[2]

[1] *University of Chinese Academy of Sciences, Beijing 100049, China*
[2] *Yunnan Observatories, Chinese Academy of Science, Kunming 650011, Yunnan, China*

Correspondence should be addressed to Zhi-ming Song; 339255245@qq.com

Received 28 March 2018; Accepted 13 August 2018; Published 12 September 2018

Academic Editor: Michael Kueppers

To expand field of view (FOV) of telescope, the method of special scanning often is used, but, for some telescopes with special structure in optics and machine, the conventional scanning methods are unsuitable. This paper proposes a novel scanning method based on autoguiding system so as to expand the FOV of fiber array solar optical telescope (FASOT) in possession of the special structure in optics and machine. Meanwhile, corresponding experiments are conducted in the FASOT prototype, FASOT-1B, in order to demonstrate that, for both FASOT and FASOT-1B, the proposed scanning method is feasible. First of all, on the basis of the software and hardware characteristics of FASOT and FASOT-1B, the three key technologies related to the proposed scanning method are described: quickly locating and pointing the first scanning step, the closed-loop controlling of multistep scanning, and the disturbance suppression of every scanning step based on Kalman filter. Afterwards, experiments are conducted and corresponding results show that the proposed scanning method is robust for the random disturbances forced on every scanning step and able to meet the scanning requirement of both FASOT and FASOT-1B .

1. Introduction

Fiber array solar optical telescope (FASOT) is a pioneer of Chinese giant solar telescope (CGST) [1], and it is a telescope which will be capable of conducting real-time, high-efficiency, high-precision spectropolarimetry of multiple magnetosensitive lines over a two-dimensional field of view, i.e., giving real-time 3D stokes measurements of multiple lines. Therefore, FASOT will act as a very efficient 3D spectropolarimeter and be capable of observing and inversing physical quantities in multiple heights of the solar atmosphere, especially the physical quantities associated with magnetic field [2, 3].

The optical path of FASOT is depicted in Figure 1. Obviously, the optical path of FASOT is different from those of general-purpose telescopes. First of all, the light from solar is collected by the guiding optics of main telescope labeled as 1 in Figure 1 and then inputted to a field stop located at the Cassegrain focus plane of main telescope that splits the FOV into two parts. One smaller part (0.5'×0.5') passes the light directly into the polarimetric system labeled as 2 in Figure 1 for the polarimetric measurement, and the remnant FOV is reflected vertically and used by the monitoring system labeled as 5 in Figure 1. Afterwards, the light modulated by the polarimeter is split into two beams with opposite polarization states (ordinary and extraordinary beams) and transmitted into integral field spectrographs and their detectors using integral field unit (IFU) with optical fibers so as to conduct two beams' spectroimaging polarimetry. Due to the compact and symmetrical optics configuration of FASOT up to the polarization modulator, the additional polarization from instrument is minimized. On the other hand, a novel polarization demodulation technique named reduced optical switching demodulation [4] is adopted by FASOT to improve the polarimetric sensitivity and reduce the integration time. These technologies mentioned above will make FASOT obtain a polarimetric noise level on the order of $8.0 \times 10^{-4} Ic$.

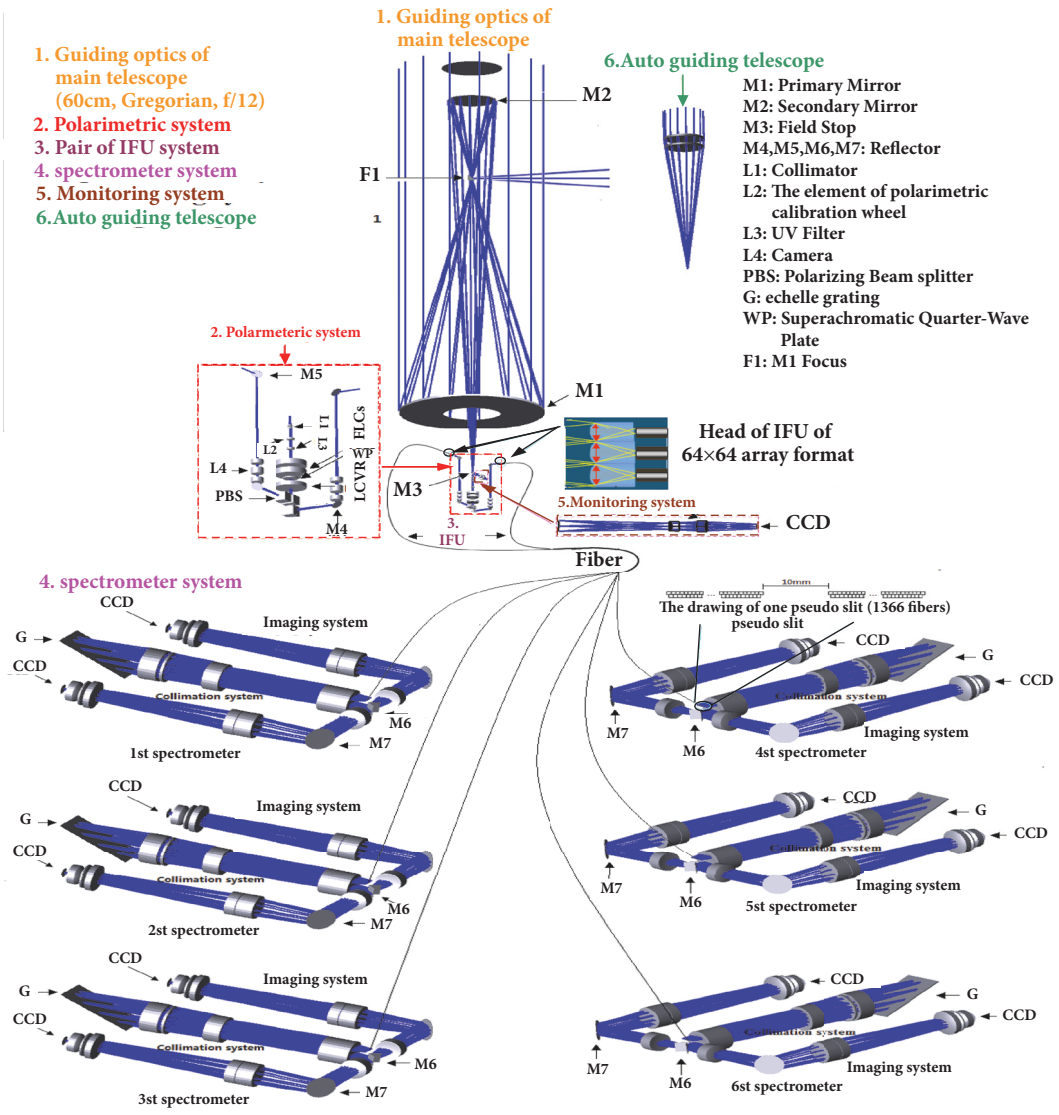

Figure 1: The optical path of FASOT.

Currently, for FASOTs, the polarimetric system and IFU labeled as 2 and 3 in Figure 1, a small FOV, 0.5'×0.5', is obtained. However, based on designing requirement, FASOT should be in possession of the ability to observe the local region of solar about 3'×3' and inverse 2D polarization spectrum image of the region. In other words, FASOT should have the capacity to scan a 2D space. However, because of the compact and symmetrical optics configuration of FASOT dedicated to improve polarimetric sensitivity, the conventional scanning methods are unsuitable for FASOT, such as the slit scanning method usually used by general-purpose telescope [5–7], the scanning method of using tip-tilt secondary mirror [8], and the method adding a rotary dual-wedge prism [9] between the secondary mirror and the field stop. Therefore, for FASOT, a special scanning method distinguishing from those mentioned above should be adopted.

Recently, a special scanning method of rotating entire telescope has been adopted by the visible infrared imaging radiometer suite (VIIRS) [10], and the method can efficiently suppresses stray light and improves polarization sensitivity. So, in consideration of the traits of FASOT, the scanning method similar to VIIRS will be adopted. But, the distinction between the two scanning methods of FASOT and VIIRS is that the method of FASOT will simultaneously rotate guiding optics, polarimetric system and autoguiding system. Furthermore, the rotation of FASOT mainly relies on the closed-loop controlling of its autoguiding system.

Normally, the autoguiding systems [11–13] used by general-purpose solar telescope just have some conventional functions such as monitoring full-disk solar image and closed-loop tracking. In contrast to those functions, FASOT will integrate the function of scanning 2D space into its conventional autoguiding system and construct a novel scanning system based on autoguiding system. It should be emphasized that the proposed scanning method has not been reported in the published literatures. What is more, some

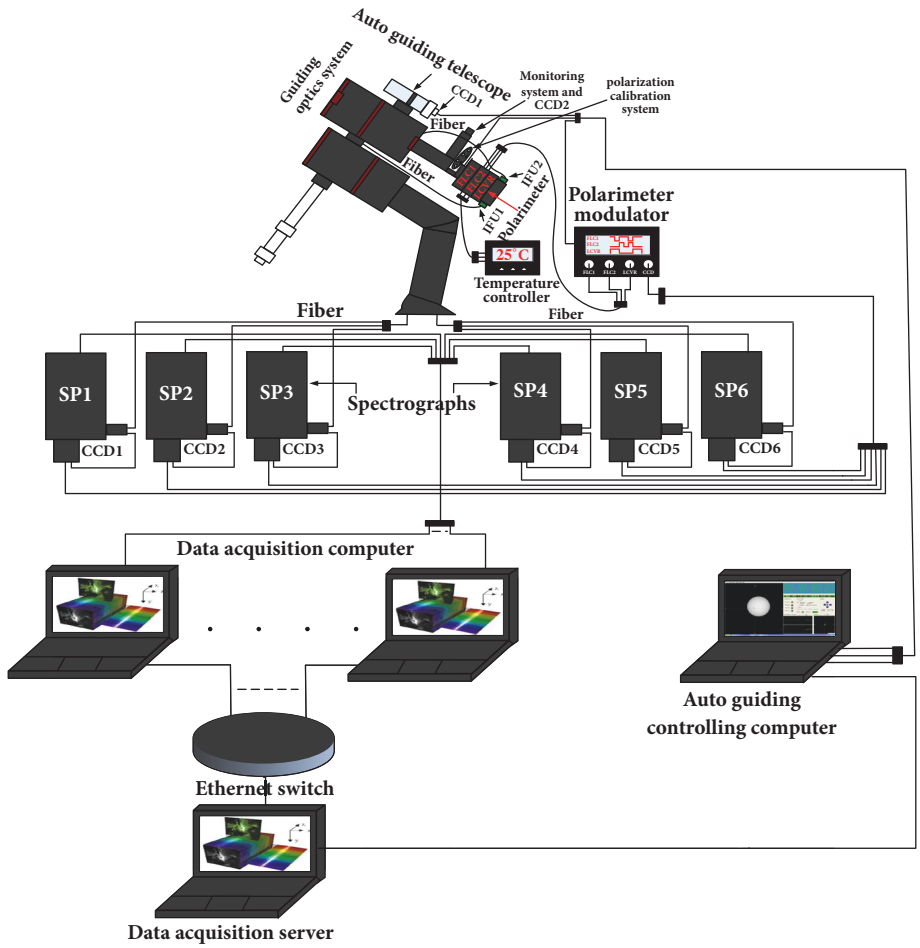

Figure 2: The structure diagram of controlling system of FASOT.

techniques used by the proposed scanning method also are novel and are not found in the published literatures. For example, in the process of multistep scanning, Kalman filter is used to suppress the random disturbances and strengthen the scanning performance. Therefore, this paper will be beneficial for the people anxious to expand the FOV of their telescope with a similar structure to FASOT.

This paper is organized as follows: Section 2 briefly introduces the structures of controlling system of FASOT and its prototype FASOT-1B and elucidates the reason why the proposed scanning system first is implemented in FASOT-1B. Section 3 describes the principle of our proposed scanning system. Three key technologies related to our proposed scanning system are introduced in Section 4 to Section 6, respectively. Experiments are conducted, and corresponding results are obtained in Section 7. The conclusions are given in Section 8.

2. Brief Introduction of FASOT and Its Prototype FASOT-1B

The structure diagram of controlling system of FASOT is shown in Figure 2. As shown in Figure 2, the system consists of the guiding optics system, autoguiding system (including autoguiding telescope, corresponding detector, and controlling computer), polarimetric system (including the polarimeter, its modulator, its temperature controller, and polarization calibration system), IFU, optical fibers, data acquisition system (including spectrographs, data acquisition computers, and server), and the mount of telescope.

In this system, autoguiding system will be taken as the central part of entire system, and besides the functions of monitoring full-disk solar image, closed-loop tracking, controlling the modulator of polarimeter, and sending the instruction of data acquisition, it also is of the capacity to scan a 2D space of local region of full-disk solar image.

It needs to be emphasized that to implement the scanning method based on autoguiding system, four conditions must be met, and they are as follows.

First, the total weight of the target object used to scan should be light, namely, a small rotary inertia. For example, For FASOT, the total weight of its guiding optics, polarimetric system, and autoguiding system is just about 120KG much less than the loading capacity of its mount, 300 Kg.

Second, the mount of telescope should have a perfect performance. For example, For FASOT, its mount is excellent in performance as a result of the fact that its tracking accuracy

Table 1: The distinctions between FASOT and its prototype FASOT-1B.

System composition	FASOT	FASOT-1B
Guiding optics system	600mm Focal length: 7200mm Field of view: 6'×6' (Gregory system)	400mm Focal length:3200mm Field of view: 2.1'×2.1' (RC system)
Aoto guiding telescope	The aperture: 80mm Focal ratio: 1:6	The aperture: 80mm Focal ratio: 1:6
Aoto guiding image sensor	SCOMS chip Resolution: 2048∗2048 Pixel size: 5.5um	SCOMS chip Resolution: 2048∗2048 Pixel size: 5.5um
The number of micro lens of IFU	2×64×64	2×11×11
The number of optical fibers	2×64×64	2×11×11
The number of spectrograph	6	1
The number of detector of the spectrographs	12	1
Data acquisition computer	6	1
Data acquisition server	1	0
The type of the mount	DDM160 of Astrosysteme Austria German equatorial mount	GM3000HSP of Micron 10 German equatorial mount
Software interface of the mount	SDK based on c/c++ and ASCOM	ASCOM
The tracking accuracy of the mount	⩽ 0.25" RMS	⩽1" RMS
The pointing accuracy of the mount	<8" RMS	<20" RMS
Polarimetric system	FASOT-1B is similar to FASOT	FASOT-1B is similar to FASOT
Loading capacity of the mount (only instrument)	300 Kg	100 Kg
The total weight of the target object used to scan	120Kg	70Kg

≤ 0.25" RMS/ 5 minutes, peak track error ≤ 0.68", and driving mode is direct-driven.

Third, the accuracy of autoguiding system should be viable. For example, for FASOT, the aperture of its autoguiding telescope is 80mm, focal ratio is 1:6, the resolution of autoguiding image sensor is 2048×2048, and pixel size is 5.5um.

Fourth, the mount of telescope should support secondary development, namely, supplying corresponding software interfaces. For example, for FASOT, its mount supports the software interfaces, such as the SDK based on C\C++ and the Astronomy Component Object Model (ASCOM).

So, on the basis of the information mentioned above, the scanning method based on autoguiding system is suitable for FASOT.

However, until now, some parts of FASOT still are in shaping. But, to ensure that the development of FASOT is smooth, a prototype of FASOT, named FASOT-1B shown in Figure 7, has been developed. The prototype is almost similar to FASOT in the optical path and the structure of control system. But some distinctions still exist between them and are displayed in Table 1. From Table 1, we can see that although the performance of the mount of FASOT-1B is not as good as the one of FASOT, it still meets the four conditions of implementing the scanning based on autoguiding system. Therefore, the proposed scanning method will first be developed and then applied to FASOT-1B. In other word, if the proposed scanning method is suitable for FASOT-1B, it must be able to be directly transported to FASOT and even has a more excellent performance as a result of that the performance of the mount of FASOT is superior to the one of FASOT-1B. Actually, This is also a good way to speed up the development of FASOT.

3. The Principle of the Proposed Scanning Method

As shown in Table 1, the software interface of the mount of FASOT-1B just supports ASCOM. Therefore, the designing of the proposed scanning method considers not only the

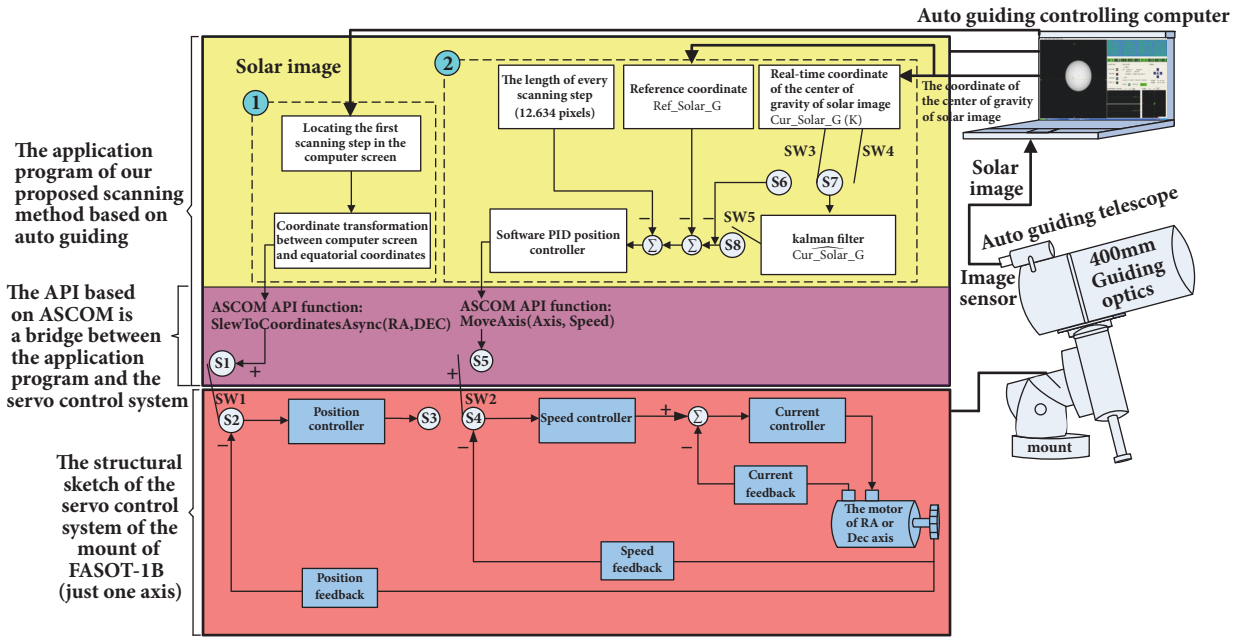

Figure 3: The software structure diagram of the proposed scanning method.

structure of the servo control system integrated into the mount of FASOT-1B, but also the relationship between the servo control system and the software interface, ASCOM. The structure diagram of combining the servo control system of the mount of FASOT-1B with its software interface to implement the proposed scanning method is shown in Figure 3. From Figure 3, we can see that the red part is the structural sketch of the servo control system of the mount of FASOT-1B, and the servo control system is a common three-ring control system, including current, speed, and position rings. The yellow parts are the software structure of our proposed scanning method integrated into the software of autoguiding system, and the purple part, ASCOM, is a bridge between the yellow part (scanning function algorithm) and the red part (servo control system).

The principle of the proposed scanning method based on autoguiding system is shown in Figure 4. The white disk is full-disk solar image acquired by autoguiding image sensor. The center point A' of yellow cross is the center of autoguiding image sensor, and it is also the optical axis of autoguiding telescope, guiding optics of FASOT-1B, polarimetric system, and IFU. Before beginning multistep scanning, telescope should be controlled and pointed to the first scanning step (in Figure 4, the first scanning step is the point B'), namely, implementing the function which quickly locates and points the first scanning step (a detailed introduction of this function will be described in Section 4. On the other hand, its software module diagram is shown in the yellow part of Figure 3 and labeled as ①). Afterwards, an entire procedure of multistep scanning will be carried out.

In Section 1, we have had the knowledge about the FOV of IFU being just 0.5'×0.5'. Therefore, to expand the FOV to 3'×3', the number of the scanning step should be equal to 35. As shown in Figure 4, the small red rectangles surrounded

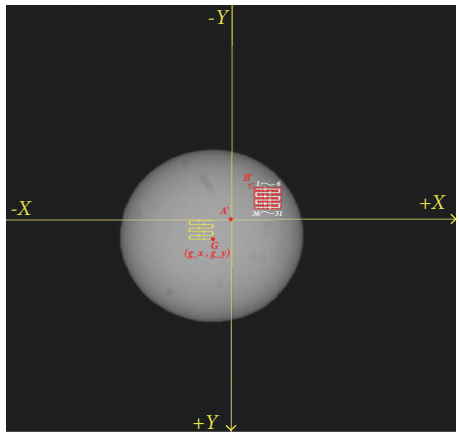

Figure 4: The principle of the proposed scanning method based on autoguiding system.

by the big one represent the corresponding positions of every scanning step, and the white arrow represents the direction of scanning. The point G(g_x,g_y) is the coordinate of the center of gravity of full-disk solar image, and the yellow arrow next to the point G(g_x,g_y) shows that the movement direction of the point G is contrary to the direction of its scanning.

Based on FASOTs, the requirements of the observation and data process, polarization modulation, and image acquisitions should be conducted after every scanning step, and then the acquired images will be reconfigured into an entire image which reflects the whole scanning areas. These requirements result in that scanning should be of the following specifications:

(1) The scanning step length should be 0.5'; namely, Ls=0.5'

(2) The accuracy between adjacent scanning steps should be less than or equal to 1"; namely, Ac≤1"

(3) The time of every scanning step should be as fast as possible

To implement the specifications mentioned above, the following strategies are adopted (a detailed software module diagram is shown in the yellow part of Figure 3 and labeled as ②).

First, as shown in Figure 3, S6 is connected by SW3, and S4 is connected to S5 by SW2.

Second, the reference coordinate of the center of gravity of full-disk solar image is calculated, **Ref_Solar_G**(**Ref_Solar_G_x**,**Ref_Solar_G_y**), before beginning every scanning step.

Third, the coordinate of the center of gravity of full-disk solar image is calculated in real-time, *Cur_Solar_G*(*k*)(*Cur_Solar_G_x*(*k*), *Cur_Solar_G_y*(*k*)), after beginning every scanning step.

Fourth, because every scanning step should meet the two specifications, Ls=0.5' and Ac≤1", when the scanning direction is horizontal X, the two errors which determine whether a horizontal scanning step was finished are calculated in real-time and expressed as

$$H\_Error\_x\,(k) = \mathbf{12.6932} - |Cur\_Solar\_G\_x\,(k) - \mathbf{Ref\_Solar\_G\_x}| \quad (1)$$

$$H\_Error\_y\,(k) = \left|Cur\_Solar\_G\_y\,(k) - \mathbf{Ref\_Solar\_G\_y}\right| \quad (2)$$

where k is the sequence number of measurement of $Cur\_Solar\_G(i)$, $i = 1 \cdots k \cdots N$, and 12.6932 is the number of pixels of a scanning step length, which corresponds to 0.5'.

Fifth, the two errors, $H\_Error\_x(k)$ and $H\_Error\_y(k)$, are sent to corresponding software PID position controllers of RA and DEC axes, respectively. Although Figure 3 just depicts one of the two axes, RA and DEC, the two axes are operated in the process of scanning simultaneously. Furthermore, $H\_Error\_x(k)$ is sent to DEC axis, and $H\_Error\_y(k)$ is sent to RA axis. On the other hand, the communication process between the two errors and the two axes depends on the Application Programming Interface (API) based on ASCOM, MoveAxis(RA or DEC,Speed).

Sixth, when both $H\_Error\_x(k)$ and $H\_Error\_y(k)$ are less than or equal to 0.4 pixels, which corresponds to 1", a scanning step of horizontal X is over. In other words, a scanning step is over as long as the terminating condition is met. Afterwards, polarization modulation and data acquisition are conducted.

Finally, for the remnant scanning steps of horizontal X, the strategies mentioned above are repeated. But, when next new scanning step starts, the reference coordinate, Ref_Solar_G, is updated again, and the coordinate, $Cur\_Solar\_G(k)$, is recalculated in real-time.

It is clear that our proposed scanning method is to combine autoguiding system with the speed ring of the servo control system (RA axis and DEC axis) in order to construct a more flexible and software-controlled close-loop controlling system.

In contrast to the direction of horizontal X, when the scanning direction is vertical Y, the two errors which determine whether a vertical scanning step was finished are calculated in real-time and expressed as follows:

$$V\_Error\_x\,(k) = |Cur\_Solar\_G\_x\,(k) - \mathbf{Ref\_Solar\_G\_x}| \quad (3)$$

$$V\_Error\_y\,(k) = \mathbf{12.6932} - \left|Cur\_Solar\_G\_y\,(k) - \mathbf{Ref\_Solar\_G\_y}\right| \quad (4)$$

Afterwards, remnant procedures are similar to those of horizontal X mentioned above.

Obviously, both $Cur\_Solar\_G\_x(k)$ and $Cur\_Solar\_G\_y(k)$ play an important role in the process of every scanning step. But they often are disturbed by wind and other factors forced on telescope (wind is dominant), resulting in that it is difficult to smoothly and steadily finish the specifications of every scanning step.

With respect to the disturbance problem, Kalman filter will be used so as to suppress the random disturbances and strengthen the robustness of every scanning step. The detailed introduction of Kalman filter will be described in Section 5.

In the end, the program flow chart of our proposed scanning method is shown in Figure 5. It needs to be emphasized that our program is based on Microsoft Foundation Classes (MFC), and multithreading and parallel processing are used for every scanning step.

4. To Quickly Locate and Point the First Scanning Step

With respect to FASOT, the destination of expanding its FOV is to observe more the solar local areas of interest. In other words, the optical axis of FASOT and its autoguiding telescope should first be pointed to a certain point, which is located within the solar local areas of interest. As shown in Figure 4, the optical axis is the point A', and the certain point located within the area of interest is B', namely, the first scanning step. Therefore, for the proposed scanning method, the first step is to move A' to B'.

Taking into consideration the fact that B' is likely to locate on any position of full-disk solar image, a Cartesian coordinate system A'XY is constructed (as shown in Figure 4, A' will be taken as the origin of the coordinate system), and then the distance between A' and B' can be obtained and expressed as the coordinate, (x,y). Afterwards, a coordinate transformation between Cartesian and equatorial coordinates will be conducted in order to obtain the equatorial coordinate of the point B' (RA,DEC), and then the API based on ASCOM, SlewToCoordinatesAsync (RA,DEC), is used to drive the FASOT's mount to move A' to B'. On the other hand, to implement the function mentioned above, as shown in

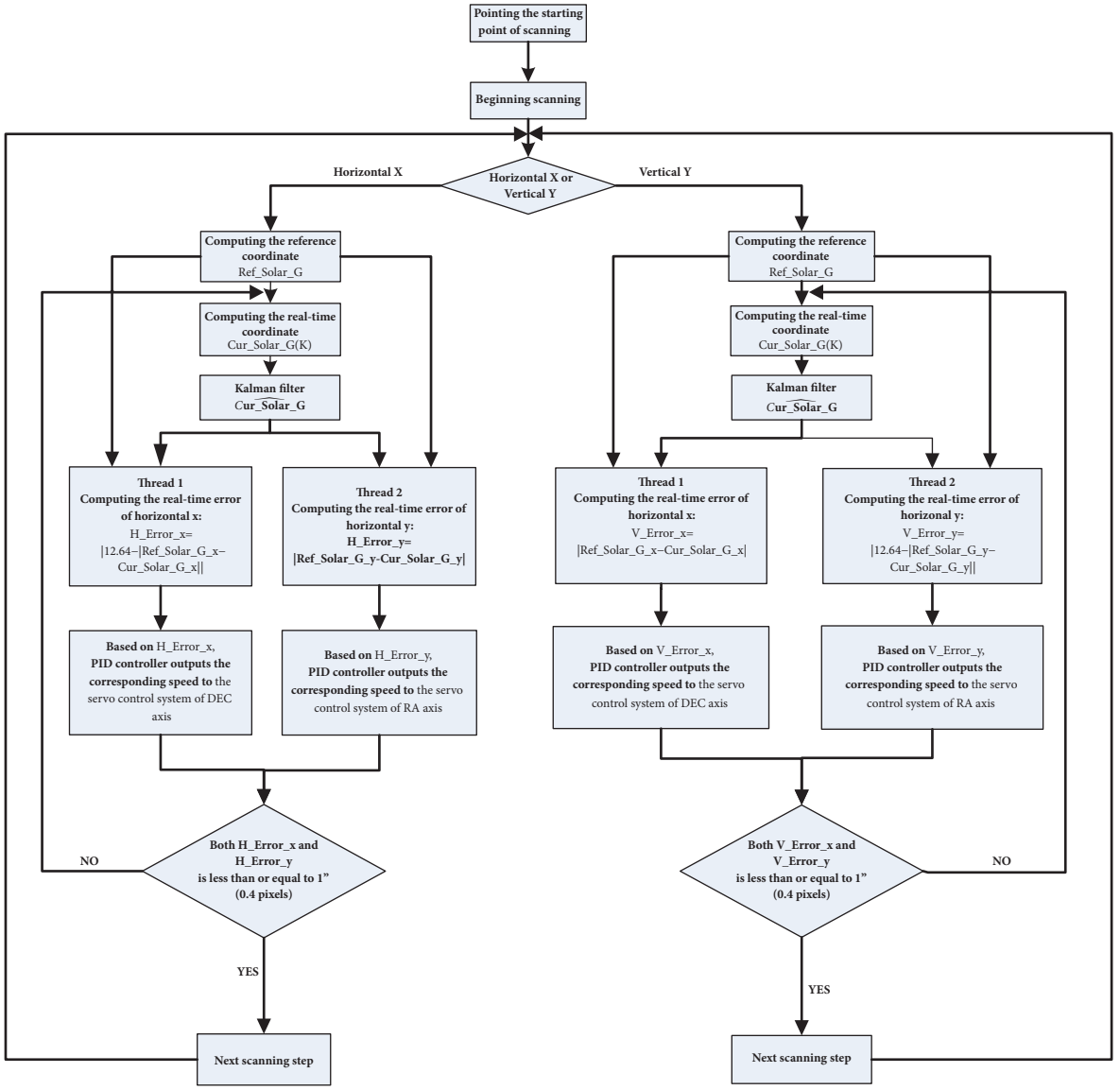

Figure 5: The program flow chart of our proposed scanning method.

Figure 3, the scanning software should first implement the following operations: connecting S1 to S2 and S3 to S4.

In the following, the coordinate transformation between Cartesian and equatorial coordinates will be described.

As shown in Figure 6, the big disk represents celestial sphere. Eq-Eq' is celestial equator. P is celestial pole. Z is zenith. O is observation site. Taking into consideration the fact that the distance between earth and solar is much larger than the diameter of earth, earth will be taken as the center of the celestial sphere, namely, the point o. 0A' is the focal length of autoguiding telescope, and its value is equal to f. A' is the center of autoguiding image sensor, and it is also the projection point of optic axis of autoguiding telescope (as shown in Figure 4, in the Cartesian coordinate system, A'XY, A' is taken as the origin of the system). A is the point located in actual solar surface currently being pointed by the optic axis of autoguiding telescope, and its equatorial coordinate is (A,D). B is another point located in actual solar surface which the optic axis of autoguiding telescope is anxious to point, and its equatorial coordinate is (A',D'). AT is the tangent line of AP, and, on the basis of AT, a Cartesian coordinates system TAT' will be constructed. It is clear that B' is the projection point of B and B", and it is also the first scanning step (as shown in Figure 4). Therefore, based on the theorems and formulas of spherical and projection triangle [14], the two transformation formulas between Cartesian and equatorial coordinates can be obtained:

$$\tan\left(A - A'\right) = \frac{y \sec\left(D\right)}{f - x \tan\left(D\right)} \tag{5}$$

$$\tan\left(D'\right) = \frac{x + f \tan\left(D\right)}{f - x \tan\left(D\right)} \cos\left(A - A'\right) \tag{6}$$

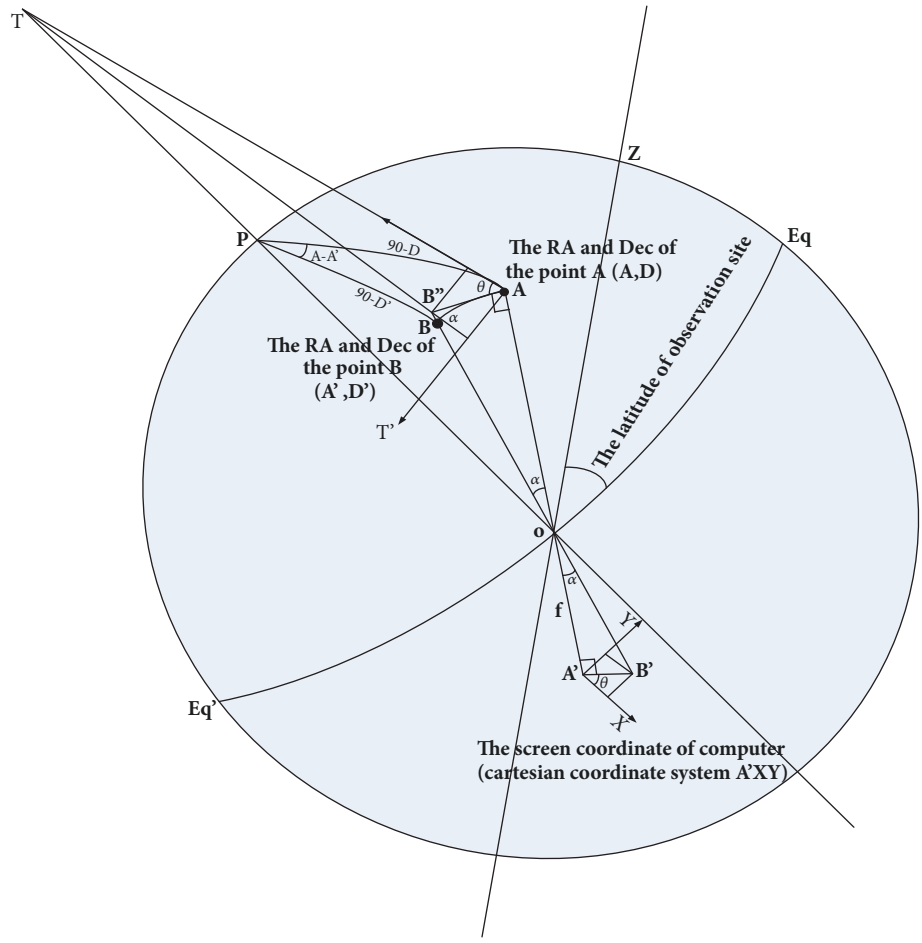

Figure 6: The coordinate transformation between Cartesian and equatorial coordinates.

where (A,D) is the equatorial coordinate of the point A currently being pointed by the optic axis of autoguiding telescope, and it is a known quantity as a result of the fact that it can be obtained through the API based on ASCOM. (x,y) is the Cartesian coordinate of the point B', and it is a known quantity as a result of the fact that it can be obtained through controlling computer screen of autoguiding system (as shown in Figure 8). f is the focal length of the autoguiding telescope, and it is also a known quantity. Therefore, based on the known quantities, the equatorial coordinate of the point B, (A',D'), can be obtained. Because B' is the projection point of B, its equatorial coordinate is also (A',D').

Obviously, this is an efficient method to quickly locate and point the first scanning step. However, this method is unsuitable for the multistep scanning described in Section 3. The reasons are as follows.

First, this method depends on the pointing accuracy of the used mount, and the accuracy often is not satisfactory. For example, as shown in Table 1, the pointing accuracy of FASOT-1B can not meet the specification of every scanning step, Ac≤1". However, with respect to the first scanning step, the pointing accuracy of FASOT-1B is sufficient as a result of the fact that it is ok as long as the first scanning step is pointed to the point which is located within the solar local area of interest.

Second, the speed regulation of this method is terrible, resulting in that after pointing every scanning step, the corresponding vibrations exists in telescope, and polarization modulation and data acquisition can not be conducted immediately. Obviously, the time of every scanning step also will be elongated as a result of waiting for the end of the vibrations.

Third, this method is not software-controlled, and its pointing procedure depends on the servo control system integrated into the mount, resulting in the fact that the movement velocity of every scanning step can not be flexibly controlled, and the capacity to resist disturbance is terrible.

5. The Closed-Loop Controlling of Every Scanning Step

As mentioned in Section 3, to meet the specifications of every scanning step, a new closed-loop controlling system combining autoguiding system with servo control system of the mount is constructed and its structure diagram is shown in Figure 3. In Section 3, the principle of this closed-loop

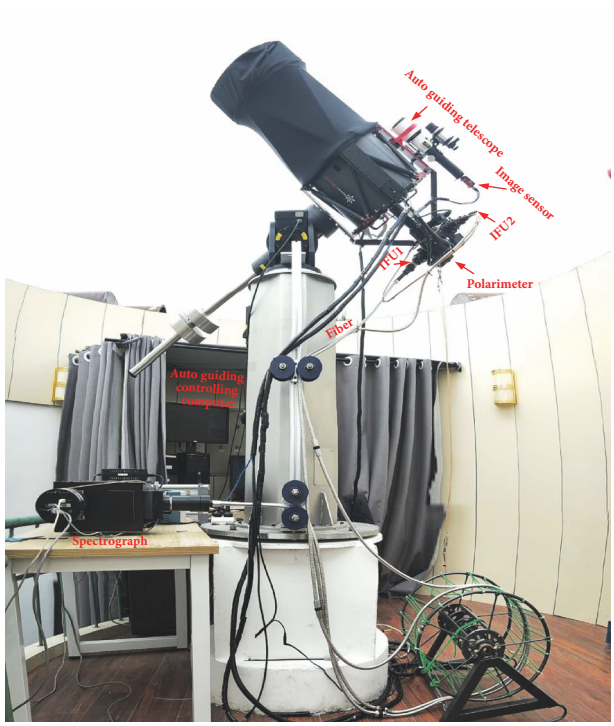

FIGURE 7: The physical map of FASOT-1B.

controlling system and its flow chart of program also have been described. Its core ideal is to construct a more flexible and software-controlled closed-loop controlling system in order to flexibly regulate the speed of every scanning step and fulfill the scanning specifications. On the other hands, it is convenient for the software-controlled closed-loop controlling system to integrate some efficient algorithms into its interior to strengthen its robustness. For example, in our scanning method, Kalman filter is used to strengthen the robustness of every scanning step.

6. Kalman Filter of Every Scanning Step

In every scanning step, due to the random disturbances from wind and other factors forced on telescope (wind is dominant), the corresponding vibrations exist in the guiding optic of main telescope, resulting in that autoguiding telescope also will be disturbed. There is no doubt that the disturbances will have a terrible influence on the performance of our multistep scanning. Therefore, corresponding measures must be taken. Kalman filter is chosen by us to improve the performance of our multistep scanning after investigating a lot of published literatures. Although Kalman filter has been applied to some telescopes and systems to strengthen their robustness [15–18], its application in telescope scanning has not been found. In the following, a detailed description about the application of Kalman filter in our scanning will be given.

Kalman filter is a statistical estimation method, which is autoregressive, linear, and unbiased. Through iteration, the optimal estimation of observation data can obtained. In other words, the disturbances forced on the observation data will be suppressed.

For our proposed multistep scanning, the application of Kalman filter is as follows.

First, for every scanning step, Kalman filter is used to obtain the optimal estimation coordinate from the real-time coordinate of the center of gravity of full-disk solar image, namely, estimating $Cur\_\widehat{Solar}\_G(k/k)$, $k = \mathbf{1},\mathbf{2}....\mathbf{N}$ from $Cur\_Solar\_G(k)$, $k = \mathbf{1},\mathbf{2}....\mathbf{N}$.

Second, $Cur\_Solar\_G(k)$ shown in (1)-(4) will be replaced by $\widehat{Cur\_Solar}\_G(k/k)$.

Finally, the remnant the procedures are similar to those described in Section 3.

The equations of traditional Kalman filter are as follows.

State and observation equations are

$$\mathbf{X}(\boldsymbol{k}) = \mathbf{A}\mathbf{X}(\boldsymbol{k}-1) + \mathbf{B}\boldsymbol{U}(\boldsymbol{k}-1) + \boldsymbol{V}(\boldsymbol{k}) \tag{7}$$

$$\mathbf{Y}(\boldsymbol{k}) = \mathbf{H}\mathbf{X}(\boldsymbol{k}) + \boldsymbol{W}(\boldsymbol{k}) \tag{8}$$

where **A** is state-transition matrix. **B** is control matrix. **V** is state noise which obeys a Gaussian distribution $N(0, {\sigma_W}^2)$. **H** is observation matrix. **W** is observation noise which obeys a Gaussian distribution $N(0, {\sigma_V}^2)$.

Time renewal equation is

$$\widehat{\mathbf{X}_1(k)} = \mathbf{A}\mathbf{X}\left(\widehat{k}-1\right) + \mathbf{B} \tag{9}$$

$$\mathbf{P}_1(k) = \mathbf{A}\mathbf{P}(k-1)\,\mathbf{A}^T + \mathbf{Q} \tag{10}$$

where **A** is state-transition matrix. **B** is control matrix. **Q** is covariance matrix of **W**.

Observation renewal equation is

$$\mathbf{K}(k) = \mathbf{P}_1(k)\,\mathbf{H}^T\left[\mathbf{H}\mathbf{P}_1(k)\,\mathbf{H}^T + \mathbf{R}\right]^{-1} \tag{11}$$

$$\widehat{\mathbf{X}(k)} = \widehat{\mathbf{X}_1(k)} + \mathbf{K}(\mathrm{k})\left[\mathbf{Y}(k) - \widehat{\mathbf{X}_1(k)}\right] \tag{12}$$

$$\mathbf{P}(k) = [\mathbf{I} - \mathbf{K}(k)\,\mathbf{H}]\,\mathbf{P}_1(k) \tag{13}$$

where **H** is observation matrix. **I** unit matrix. **K** is Kalman gain. **R** is covariance matrix of **V**. $\widehat{\mathbf{X}(k)}$ is the estimation value of Kalman filter.

Obviously, on the basis of the equations mentioned above, the scanning state and observation equations (7)-(8) are first constructed. Afterwards, the matrixes mentioned above, (**A**, **B**, **H**, **W**, **Q**, **V**, and **R**), are obtained. Next, the estimation data of Kalman filter, $\widehat{\mathbf{Cur\_Solar}}\_\mathbf{G}(k/k)$, is calculated by iteration equations (9)-(13). It needs to be emphasized that in our proposed multistep scanning, the scanning direction contains horizontal X and vertical Y. Therefore, different scanning direction has its own state and observation equations.

Taking the scanning of horizontal X for example, the scanning procedure is that the RA axis and DEC axis are simultaneously operated based on the two errors, H_Error_x and H_Error_y. Furthermore, this operation results in the change of the real-time coordinate of the center of gravity of full-disk solar image, $Cur\_Solar\_G(k)$, at the same movement size and speed as the two axes. Therefore, the scanning

movement equation of $Cur\_Solar\_G(k)$, namely, its state equation, can be expressed as follows:

$$\begin{bmatrix} \boldsymbol{X}_{\mathbf{S}}(\boldsymbol{k}) \\ \boldsymbol{X}_{\mathbf{V}}(\boldsymbol{k}) \end{bmatrix} = \begin{bmatrix} 1 & \boldsymbol{T} \\ 0 & \boldsymbol{T} \end{bmatrix} \begin{bmatrix} \boldsymbol{X}_{\mathbf{S}}(\boldsymbol{k}-1) \\ \boldsymbol{X}_{\mathbf{V}}(\boldsymbol{k}-1) \end{bmatrix} + \begin{bmatrix} \dfrac{1}{2\boldsymbol{T}^2} \\ \boldsymbol{T} \end{bmatrix} \boldsymbol{U}(\boldsymbol{k}-1) + \boldsymbol{V}(\boldsymbol{k}) \tag{14}$$

where k is the sequence number of measurement of $Cur\_Solar\_G(i)$, $i = 1 \cdots k \cdots N$, and T is its measurement cycle. $X_{\mathbf{S}}(k)$ is the movement size of $Cur\_Solar\_G(k)$. $X_V(k)$ is the movement speed of $Cur\_Solar\_G(k)$. $U(k)$ is the movement acceleration of $Cur\_Solar\_G(k)$. $\boldsymbol{V}(\boldsymbol{k})$ is the random disturbances enforced on telescope, and suppose that it obeys the Gaussian distribution $N(0,{\sigma_V}^2)$.

On the other hand, the scanning observation equation can be expressed as follows:

$$\begin{bmatrix} \boldsymbol{Y}_{\mathbf{S}}(\boldsymbol{k}) \\ \boldsymbol{Y}_{\mathbf{V}}(\boldsymbol{k}) \end{bmatrix} = \begin{bmatrix} 1 & 0 \end{bmatrix} \begin{bmatrix} \boldsymbol{X}_{\mathbf{S}}(\boldsymbol{k}) \\ \boldsymbol{X}_{\mathbf{V}}(\boldsymbol{k}) \end{bmatrix} + \boldsymbol{W}(\boldsymbol{k}) \tag{15}$$

where Y_S(k) and Y_V(k) are the observation data of autoguiding image sensor for $X_{\mathbf{S}}(k)$ and $X_V(k)$. $\boldsymbol{W}(\mathbf{k})$ is observation noise of autoguiding image sensor, and suppose that it obeys a Gaussian distribution $N(0,{\sigma_W}^2)$.

Due to the fact that $Cur\_Solar\_G(k)$ consists of $Cur\_Solar\_G\_x(k)$ and $Cur\_Solar\_G\_y(k)$, therefore, (14) and (15) can be expanded as follows:

$$\begin{bmatrix} \mathbf{X}_{\mathbf{S\_X}}(\boldsymbol{k}) \\ \mathbf{X}_{\mathbf{V\_X}}(\boldsymbol{k}) \\ \mathbf{X}_{\mathbf{S\_Y}}(\boldsymbol{k}) \\ \mathbf{X}_{\mathbf{V\_Y}}(\boldsymbol{k}) \end{bmatrix} = \begin{bmatrix} \mathbf{1} & \mathbf{T} & 0 & 0 \\ 0 & 1 & 0 & 0 \\ 0 & 0 & 1 & \mathbf{T} \\ \mathbf{0} & \mathbf{0} & \mathbf{0} & \mathbf{1} \end{bmatrix} \begin{bmatrix} \mathbf{X}_{\mathbf{S\_X}}(\boldsymbol{k}-1) \\ \mathbf{X}_{\mathbf{V\_X}}(\boldsymbol{k}-1) \\ \mathbf{X}_{\mathbf{S\_Y}}(\boldsymbol{k}-1) \\ \mathbf{X}_{\mathbf{V\_Y}}(\boldsymbol{k}-1) \end{bmatrix} + \begin{bmatrix} \dfrac{\mathbf{1}}{\mathbf{2T^2}} \\ \mathbf{T} \\ \dfrac{\mathbf{1}}{\mathbf{2T^2}} \\ \mathbf{T} \end{bmatrix} \boldsymbol{U}(\boldsymbol{k}-1) + \boldsymbol{V}(\boldsymbol{k}) \tag{16}$$

$$\begin{bmatrix} \mathbf{Y}_{\mathbf{S}}(\boldsymbol{k}) \\ \mathbf{Y}_{\mathbf{V}}(\boldsymbol{k}) \end{bmatrix} = \begin{bmatrix} 1 & 0 & 0 & 0 \\ 0 & 0 & 1 & 0 \end{bmatrix} \begin{bmatrix} \mathbf{X}_{\mathbf{S\_X}}(\boldsymbol{k}) \\ \mathbf{X}_{\mathbf{V\_X}}(\boldsymbol{k}) \\ \mathbf{X}_{\mathbf{S\_Y}}(\boldsymbol{k}) \\ \mathbf{X}_{\mathbf{V\_Y}}(\boldsymbol{k}) \end{bmatrix} + \boldsymbol{W}(\boldsymbol{k}) \tag{17}$$

Obviously, from the two equations, (16) and (17), we can obtain the state-transition matrix **A**, the control matrix **B**, and the observation matrix **H**. Generally, $\boldsymbol{V}$ is associated with the disturbances forced on telescope in the procedure of scanning movement, and $\boldsymbol{W}$ is related to the noise of autoguiding image sensor. However, in our scanning movement, autoguiding telescope and its image sensor are located on the top of the guiding optics of main telescope (as shown in the Figure 7). Therefore, the disturbances forced on telescope will have a similar influence on autoguiding telescope and its image sensor. In other words, the disturbances can be observed by autoguiding system and seen as the noise of autoguiding image sensor. On the basis of the above analysis, in our Kalman filter equation (16), $\boldsymbol{V}$ can be seen as a very small quantity or zero, and in (17), $\boldsymbol{W}$ can be seen as the accumulation of the disturbances forced on telescope and autoguiding image sensor's own noise.

On the other hand, we have had the knowledge that, for **W**, the influence of wind is dominant. What is more, different levels of wind result in different **W**. Furthermore, our scanning will be stopped when the level of wind is stronger than level three wind. Therefore, in different levels of wind (from level one to level three), three groups of the real-time coordinates of the center of gravity of full-disk solar image are obtained, namely, $Cur\_Solar\_G\_1$, $Cur\_Solar\_G\_2$, and $Cur\_Solar\_G\_3$. In the meantime, based on the three groups of coordinates, three groups of **W** will be obtained, namely, **W**1, **W**2, and **W**3. Finally, when the Kalman filter method mentioned above is applied to our every scanning step of horizontal X, the different **W** will be selected based on corresponding the level of wind.

With respect to the scanning of vertical Y, the strategies about using Kalman filter are similar to the one of horizontal X mentioned above.

In the end, the things which we need to point to are as follows.

First, as shown in Figure 3, when Kalman filter is used, S4 is connected to S5 by SW2, S7 is connected by SW3, and S8 is connected by SW5.

Second, the level of wind is determined by the speed of wind, and the relationship between them is shown in Table 2. Furthermore, a digital anemometer is used by us to measure the speed of wind and select different **W** in the procedure of scanning.

7. Experiments and Results of Scanning

To demonstrate whether the proposed scanning method can meet its specifications ((1) the scanning step length should be 0.5'; (2) the accuracy between adjacent scanning steps should be less than or equal to 1"; (3) the time of every scanning step should be as fast as possible), experiments have been conducted in FASOT prototype FASOT-1B. Because the performance of the mount of FASOT is superior to the one of FASOT-1B, if the scanning specifications can be met by FASOT-1B, then they also can be did by FASOT. Figure 7 displays the picture of real product of FASOT-1B, and Figure 8 displays the graphical user interface of controlling system of our proposed scanning method based on autoguiding system on the computer screen.

Because our proposed scanning method is based on the real-time error of the center of gravity of full-disk solar image, the trajectory of the center of gravity of full-disk solar image can be used to verify whether every scanning step is smooth and accurate. In the meantime, the trajectory also can be

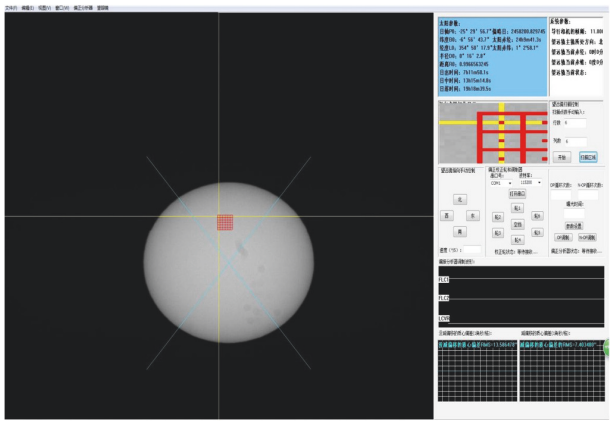

Figure 8: The graphical user interface of controlling system of our proposed scanning method based on autoguiding system on the computer screen.

Table 2: The relationship between the level of wind and speed of wind.

The level of wind	The speed of wind (m/s)
1	0.3-1.6
2	1.6-3.4
3	3.4-5.5

used to verify whether the scanning specifications can be met.

First of all, we need to verify whether the Kalman filter can strengthen the robustness of every scanning step or not. Therefore, the structure of Figure 3 should be that S5 is connected to S4 by SW2, SW3 is connected to S6, SW4 is connected to S7, and SW5 is not connected to S8. In other words, the estimated data of Kalman filter, $\widehat{\text{Cur\_Solar\_G}}(k/k)$, just is taken as a comparison variable with Cur_Solar_G(k), instead of a feedback variable. Therefore, in distinct levels of wind (from level one to level three), some experiments have been conducted, and corresponding data also has been obtained. To better show the performance of Kalman filter, the group of data with remarkable random disturbances, which is obtained in level 3 wind, is used and displayed in Figure 9. From Figure 9(b), it is clear that the center of gravity of full-disk solar image without Kalman filter (the black line shown in Figure 9(b)) will be off its trajectory when some strong random disturbances exist in the process of scanning. In contrast to the result without Kalman filter, the center of gravity of full-disk solar image with Kalman filter (the red line shown in Figure 9(b)) almost keeps its trajectory. What is more, compared with the trajectory without Kalman filter, the one with Kalman filter is more smooth and steady. Therefore, we can conclude that Kalman filter can correctly estimate the position of the center of gravity of full-disk solar image, and if the output of Kalman filter, $\widehat{\text{Cur\_Solar\_G}}(k/k)$, can be applied to the closed-loop control system of our proposed scanning method, our proposed scanning method will be of more strong performance.

Second, the Kalman filter is applied to the closed-loop controlling system of our proposed scanning method (the structure of Figure 3 should be that S5 is connected to S4 by SW2, SW3 is connected to S7, and SW5 is connected to S8). Afterwards, some experiments similar to those mentioned above also have been conducted, and then the group of data with remarkable random disturbances, which is obtained in level 3 wind, is used and displayed in Figure 10.

Because, currently, the Kalman filter has been used, the scanning procedure should be smooth and steady. Therefore, the movement accuracy and time between adjacent scanning steps are what we want to obtain. With respect to the accuracy, if the number of pixels between adjacent scanning steps is within the range $[12.2932, 12.6932]$, the accuracy of every scanning step can be met. Therefore, in Figure 10(b), the trajectory of the center of gravity of full-disk solar image just contains points, which belong to the beginning and end of every scanning step. Based on Figure 10(b), accuracy of every scanning step can be obtained, and it is clear that their accuracy are satisfactory. On the other hand, to obtain the movement time of every scanning step, the timer based software is used, and corresponding results show that all their time is less than or equal to 4s.

Finally, the method of quickly locating and pointing the first scanning step described in Section 4 is also tested, and results show that the first scanning step always is pointed to the point, which is located within the solar local area of interest.

Obviously, from the analyses mentioned above, we may come to the conclusion that, for FASOT-1B, the proposed scanning method can meet the specifications of every scanning step. In other words, this method can be directly transplanted to FASOT after it is built.

8. Conclusion

On the basis of the special structure of FASOT in optics and machine, this paper proposes a novel scanning method based on autoguiding system so as to expand the field of view of observation of FASOT. In the meantime, the proposed scanning method also is turned out to be feasible in the FASOT prototype FASOT-1B. In other words, this method can be directly transplanted to FASOT after it is built. On the other hand, in addition to giving a detailed introduction to the principle of our proposed scanning method, this paper also provides an efficient method based on Kalman filter to suppress the random disturbances forced on every scanning step so as to strengthen the scanning performance.

As a closing remark, because FASOT has a special structure which is distinct from the existing solar telescopes and our proposed scanning method based on autoguiding system has not been reported in the published literatures, the key technologies described in our proposed scanning method are able to be taken as an efficient reference when the solar telescopes with a similar structure to FASOT are constructed, especially in the situation where the mount of the solar telescopes supports the software protocols based on ASCOM.

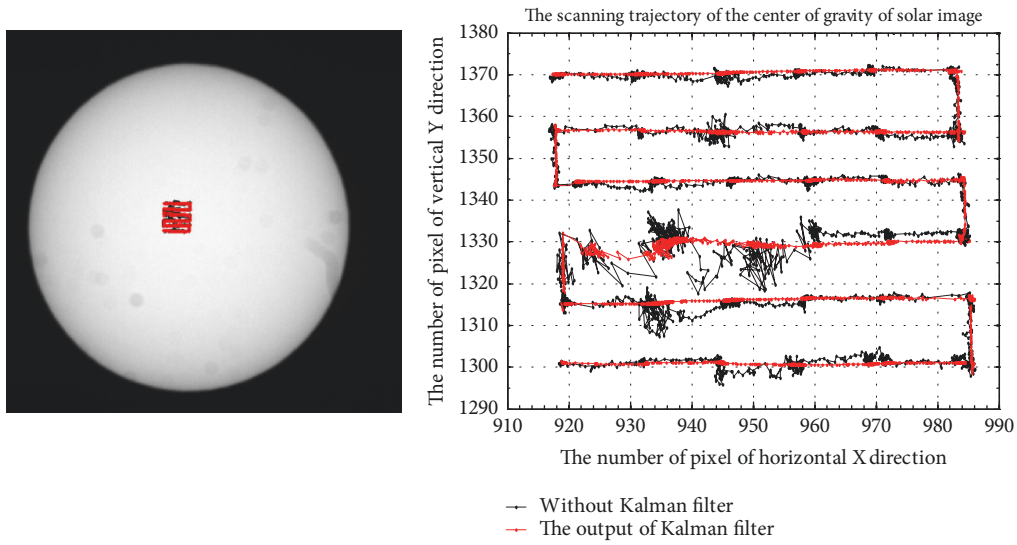

(a) The track of the actual picture (b) The track of multistep scanning with and without Kalman filters

Figure 9: The comparison of the track of the center of gravity of full-disk solar image.

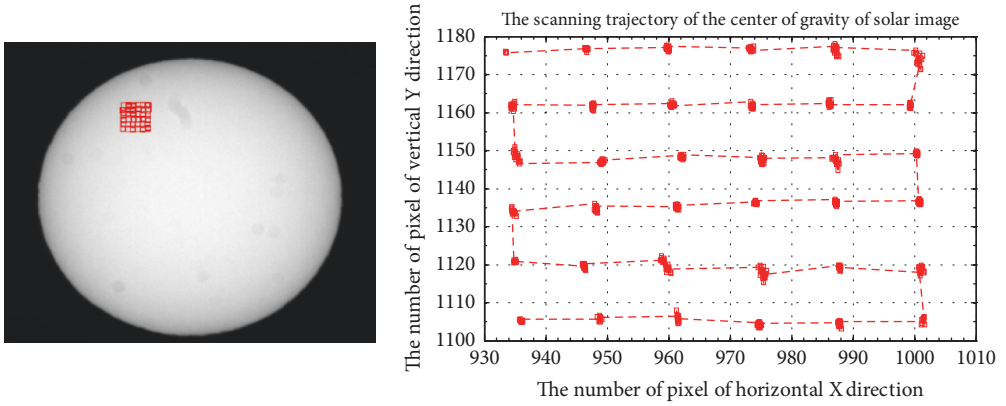

(a) The actual scanning position (b) The track of multistep scanning using Kalman filter

Figure 10: The track of the center of gravity of full-disk solar image using Kalman filter.

Data Availability

The data used to support the findings of this study are available from the corresponding author upon request.

Conflicts of Interest

The authors declare that they have no conflicts of interest.

Acknowledgments

This work is supported by the National Natural Science Foundation of China (Grant nos. 11527804 and 11703087)

References

[1] Y. Deng, Z. Liu, and C. Group, "The Chinese Giant Solar Telescope (CGST)," in *Proceedings of the Second ATST-EAST Meeting: Magnetic Fields from the Photosphere to the Corona*, 2012.

[2] G. T. Dun and Z. Q. Qu, "Design of the polarimeter for the fibre arrayed solar optical telescope," *Acta Astronomica Sinica*, vol. 53, no. 1, pp. 342–352, 2012.

[3] Z. Q. Qu, "A fiber arrayed solar optical telescope," in *Proceedings of the Conference Series of Astronomical Society of the Pacific*, vol. 437, pp. 423–431, 2011.

[4] Z. Q. Qu, G. T. Dun, L. Chang et al., "Spectro-imaging polarimetry of the local corona during solar eclipse," *Solar Physics*, vol. 292, no. 2, p. 37, 2017.

[5] Y. Changchun, L. Zhenggang, C. Yuchao, and X. Jun, "The design of a spectrum scanning observation system for the new vacuum solar telescope," *Astronomical Research and Technology*, vol. 13, no. 2, pp. 257–265, 2016.

[6] F. F. Yue, X. U. Jun, and R. L. Zhang, "Analysis of the slit-scanning control system of the 1 meter solar telescope of YNAO," *Astronomical Research & Technology*, vol. 6, no. 4, pp. 319–326, 2009.

[7] K. Ichimoto, B. Lites, D. Elmore et al., *Polarization Calibration of the Solar Optical Telescope Onboard Hinode*, The Hinode Mission, Springer, NY, USA, 2008.

[8] C. Pernechele, F. Bortoletto, and K. Reif, "Position control for active secondary mirror of a two-mirror telescope," *Telescope Control Systems II. International Society for Optics and Photonics*, vol. 3112, pp. 172–181, 1997.

[9] Z. Jingguo, L. Feng, and H. Qitai, "Design and realization of an airborne LiDAR dual-wedge scanning system," *Infrared and Laser Engineering*, vol. 45, no. 5, 2016.

[10] R. E. Wolfe, G. Lin, M. Nishihama et al., "Suomi NPP VIIRS prelaunch and on-orbit geometric calibration and characterization," *Journal of Geophysical Research: Atmospheres*, vol. 118, no. 20, 2013.

[11] C. H. Wu and Q. S. Zhu, "The tracking and guiding method for full solar disk vector magnetograph telescope," *Astronomical Research & Technology*, vol. 4, no. 2, p. 147, 2007.

[12] W. Thompson and M. Carter, "EUV full-sun imaging and pointing calibration of the SOHO/CDS," *Solar Physics*, vol. 178, no. 1, pp. 71–83, 1998.

[13] X. Jiang, H. U. Ke-Liang, and J. B. Lin, "Tracking and guiding for full solar disk image using large CCD-array," *Optics & Precision Engineering*, vol. 16, no. 9, pp. 1589–1594, 2008.

[14] L. G. Taff, *Computational Spherical Astronomy*, Wiley, 1981.

[15] Y. Yang, N. Rees, and T. Chuter, "Reduction of encoder measurement errors in UKIRT telescope control system using a Kalman filter," *IEEE Transactions on Control Systems Technology*, vol. 10, no. 1, pp. 149–157, 2002.

[16] T. Erm and S. Sandrock, "Adaptive periodic error correction for the VLT," in *Proceedings of the Large Ground-based Telescopes (International Society for Optics and Photonics)*, pp. 900–909, 2003.

[17] T. Erm and S. Sandrock, "Adaptive correction of periodic errors improves telescope performance," in *Proceedings of the 2005 IEEE American Control Conference*, vol. 6, pp. 3776-3777, 2005.

[18] N. Tian, J. Sun, and Z. Liu, "Real-time light-spot positioning for target observation and aiming based on monocular vision," *Infrared & Laser Engineering*, 2014.